Structural Engineering and Mechanics, *Vol. 71, No. 1 (2019) 099-107*
DOI: https://doi.org/10.12989/sem.2019.71.1.099

Wave dispersion characteristics of porous graphene platelet-reinforced composite shells

Farzad Ebrahimi*[1], Ali Seyfi[1], Ali Dabbagh[2] and Francesco Tornabene[3]

[1]*Department of Mechanical Engineering, Faculty of Engineering, Imam Khomeini International University, Qazvin, Iran*
[2]*School of Mechanical Engineering, College of Engineering, University of Tehran, Tehran, Iran*
[3]*Department of Civil, Chemical, Environmental, and Materials Engineering, University of Bologna, Bologna, Italy*

(Received February 28, 2019, Revised March 16, 2019, Accepted March 20, 2019)

Abstract. Wave propagation analysis of a porous graphene platelet reinforced (GPLR) nanocomposite shell is investigated for the first time. The homogenization of the utilized material is procured by extending the Halpin-Tsai relations for the porous nanocomposite. Both symmetric and asymmetric porosity distributions are regarded in this analysis. The equations of the shell's motion are derived according to Hamilton's principle coupled with the kinematic relations of the first-order shear deformation theory of the shells. The obtained governing equations are considered to be solved via an analytical solution which includes two longitudinal and circumferential wave numbers. The accuracy of the presented formulations is examined by comparing the results of this method with those reported by former authors. The simulations reveal a stiffness decrease in the cases which porosity influences are regarded. Also, one must pay attention to the effects of longitudinal wave number on the wave dispersion curves of the nanocomposite structure.

Keywords: wave propagation; porous nanocomposite; graphene platelet (GPL); first-order shear deformation shell theory

1. Introduction

To ameliorate the mechanical properties of homogeneous materials, it is common to employ a set of reinforcing elements dispersed in a matrix via both uniform and functionally graded (FG) distribution patterns. Previously, only macrofillers were implemented to be dispersed in an initial media; however, the outstanding mechanical properties of the nanosize elements were appealing enough in the researchers' point of view to design composites made from inserting nanofillers in either polymeric or metallic matrices. Due to the implementation of nanofillers in such a novel type of materials, they are usually called nanocomposites. The most famous nanofillers are carbon nanotubes (CNTs), boron nitride nanotubes (BNNTs) and graphene platelets (GPLs). The remarkable stiffness enhancement, generated from dispersing nanofillers inside a matrix, attracted a large number of authors to investigate the mechanical characteristics of nanocomposites. Plus, due to great capability and superb properties of these materials, specifically, GPLs reinforced nanocomposite, they are utilized in various engineering fields such as the automotive industry, aerospace engineering, and civil constructions.

For instance, Ke *et al*. (2010) analyzed the nonlinear vibrational answers of CNT reinforced (CNTR) nanocomposite beams. Finite element method (FEM) is combined with the Mindlin plate theory in order to investigate the static and dynamic characteristics of CNTR nanocomposites (Zhu *et al*. 2012). Ansari *et al*. (2014) probed the nonlinear externally motivated dynamic responses of CNTR nanocomposite beams. Moreover, Shen and Xiang (2014) studied the thermal postbuckling problem of CNTR nanocomposite shells rested on an elastic medium. The nonlinearity effects are again considered in another research dealing with the bending behaviors of CNTR nanocomposites within the framework of a FEM based approach Zhang *et al*. (2015). Civalek (2017) developed an efficient numerical method for the goal of solving the vibration problem of plates and shells reinforced with CNTs. Some efforts are made by researchers to investigate the thermo-mechanical behaviors of shallow shells consisted of CNTR nanocomposites (Wang *et al*. 2017, Rout and Karmakar 2018).

On the other hand, nanocomposite structures differ from micro- and nano-scale elements which the classical continuum theory does not apply for them. Evidently, analyzing of nanostructures is the lucrative issue that lots of investigations have been carried out by many researchers. Kocaturk and Akbas (2013) employed MCST to examine wave dispersion behavior of a cantilever microbeam subjected to impact force. Akgöz and Civalek (2014) investigated buckling analysis of microbeams by applying MSGT on basis of sinusoidal beam model. Pour *et al*. (2015) discussed the nonlinear vibration analysis of SWCNT based upon nonlocal sinusoidal shear deformation beam theory. The buckling and bending responses of simply supported microbeams resting on an elastic foundation based on MSGT are reported by Akgöz and Civalek

*Corresponding author, Professor
E-mail: febrahimy@eng.ikiu.ac.ir

ISSN: 1225-4568 (Print), 1598-6217 (Online)

(2015b). Akgöz and Civalek (2015a) further studied mechanical characteristics of microplate based on MSGT and utilizing sinusoidal plate model. Ebrahimi and Barati (2017a) analyzed magnetic field effect on wave propagation of FG nano-sized beams resting on an elastic substrate in the framework of NSGT. In another attempt, Ebrahimi and Dabbagh (2017b) researched wave dispersion responses of FG piezoelectric nanobeams by regarding porosity and angular velocity effects. Thermal stability behavior of FG nanoplates rested on elastic medium in thermal environments is studied by Khetir *et al*. (2017). On the basis of NSGT, wave propagation analysis of FG nanoscale beam exposed to thermal loading and rotating influence is surveyed by Ebrahimi *et al*. (2017). Also, Ebrahimi and Barati (2017b) probed free vibration answers of FG nanobeams subjected to the non-uniform axial magnetic field in the framework of NSGT. Moreover, NSGT is applied by Ebrahimi and Dabbagh (2017a) in order to influence of rotation on wave propagation responses of rotating magneto-electro-elastic (MEE) nanoplates. Bending behavior of an edge cracked cantilever FG nanobeam under transversal load on the basis of MCST is presented by Akbaş (2018). Ebrahimi *et al*. (2018) discussed wave propagation analysis of a rotating FG nanobeam using Eringen's nonlocal elasticity theory. Moreover, Ebrahimi and Barati (2018) explored the vibrational behavior of curved FG piezoelectric nano-scale beams based upon NSGT. Ebrahimi *et al*. (2019) recently examined the influence of magnetic and electric field on wave dispersion analysis of MEE nanotube subjected to thermal loading on the basis of Eringen's nonlocal theory. In addition, there are several investigations that have analyzed mechanical behavior of macro structures which made of different materials such as FG material. For example, Zidi *et al*. (2017) explored the vibration and bending characteristics of FG beams HSDT. The nonlinear postbuckling characteristics of simply supported deformable symmetric composite beams using HSDT is carried out by Kaci *et al*. (2018).

In the past few years, lots of authors devoted their time to analyze the mechanical behaviors of GPL reinforced (GPLR) nanocomposites once the structures are subjected to various external loadings. In order to earn more data about the procured valuable researches in this field, the most crucial papers in this area will be reviewed in the following. Kitipornchai *et al*. (2017) investigated both static and dynamic mechanical behaviors of GPLR nanocomposite beams. The nonlinearity effects are covered by Feng *et al*. (2017b) studying the vibrational responses of FG-GPLR nanocomposite beams. The same authors have also performed another nonlinear analysis on the deflection characteristics of nanocomposite beams reinforced with graded distributions of GPLs Feng *et al*. (2017a). Furthermore, Song *et al*. (2017a) analyzed the vibration problem of GPLR nanocomposite plates with both natural and forced excitations. The issue of stability analysis of a GPLR sandwich nanocomposite plate is surveyed by Song *et al*. (2017b) while a biaxial compression is assigned to the structure. In another attempt, both pre- and post-buckling analyses are performed by Yang *et al*. (2017) on the GPLR nanocomposite multi-layered beams. In addition, Zhao *et al*. (2017) probed dynamic fluctuation and deflection features of GPLR nanocomposite plates with a non-uniform cross-section. In the noted investigations, the porosity effect which has a considerable influence on the mechanical behavior of structures, aren't regarded. In some of the studies and present paper, this effect is explored. Barati and Zenkour (2017) considered for the porosity effects in a paper dealing with the post-buckling responses of a GPLR nanocomposite beam. The vibration problem of a nanocomposite shell, reinforced with GPLs, is solved by Barati and Zenkour (2018b) with respect to the influences of porosity. Also, the same authors have analyzed the post-buckling characteristics of GPLR nanocomposites by considering the geometrical imperfections as well as porosity (Barati and Zenkour, 2018a). Reddy *et al*. (2018) presented a general FEM based model to observe the vibrational responses of GPLR nanocomposite plates with various edge supports. Both stability and deflection analyses of GPLR nanocomposite plates were procured by Song *et al*. (2018). A group of buckling analyses was carried out by Wang and his colleagues on the cylindrical shells consisted of GPLR nanocomposites (Wang *et al*. 2018b, Wang *et al*. 2018d, Wang *et al*. 2018c). Lately, Wang *et al*. (2018a) surveyed both bending and vibration problems of GPLR nanocomposite shells.

To the best of the authors' consciousness, there are many valuable types of research going through the bending, buckling and vibration problems of cylindrical shells made from GPLR nanocomposites. However, no paper can be found dealing with the wave propagation problem of such an element. Wave propagation analysis is one of the important analysis methods that can be very fruitful in fault detection. Due to this deficiency, we are about to analyze this problem in the present paper within the framework of an analytical wave solution by considering the porosity effects. In other words, in this study, the effect of two porosity distributions on wave propagation analysis of the GPLR nanocomposite shell is investigated. The Navier equations of the shell will be derived according to the dynamic form of the principle of virtual work incorporated with the strain-displacement equations of the first-order shear deformation shell theorem. The presented results indicate that the porous cylinders provide lower phase speeds for the dispersed waves in comparison with the perfect ones.

2. Theory and formulations

2.1 Homogenization procedure

In this section, the Halpin-Tsai model is introduced to describe the equivalent mechanical properties of the GPLR beams. Consider a cylinder as shown in Fig. 1 which is consisted of porous GPLR nanocomposite. The porosities can be in the material with both uniform and non-uniform distribution patterns. In the following formulations, the homogenization will be discussed on the basis of symmetric and asymmetric distributions. The mechanical properties of a porous nanocomposite shell can be computed in the

following form:

$$E(z)=E_1\left(1-e_0\lambda(z)\right),$$
$$G(z)=\frac{E(z)}{2(1+\nu(z))}, \quad (1)$$
$$\rho(z)=\rho_1\left(1-e_m\lambda(z)\right)$$

where $\lambda(z)$ is the function which determines the porosity distribution through the thickness of the structure. this function can be formulated in the following form for symmetric and asymmetric distribution patterns for the porous nanocomposite:

$$\lambda(z)=\cos\left(\frac{\pi z}{h}\right) \quad \text{for symmetric distribution}$$
$$\lambda(z)=\cos\left(\frac{\pi z}{2h}+\frac{\pi}{4}\right) \quad \text{for asymmetric distribution} \quad (2)$$

Also, E_1, G_1, and ρ_1 are the maximum amounts of elasticity modulus, shear modulus and mass density in the nanocomposite, respectively. Besides, e_0 and e_m are the porosity and mass density coefficients, respectively. These variants can be calculated as:

$$e_0=1-\frac{E_2}{E_1}=1-\frac{G_2}{G_1},$$
$$e_m=\frac{1.121\left[1-\sqrt[2.3]{1-e_0\lambda(z)}\right]}{\lambda(z)} \quad (3)$$

The Poisson's ratio of a porous GPLR nanocomposite material can be formulated in the following form:

$$\nu(z)=0.221\tilde{p}+\nu_1\left(0.342\tilde{p}^2-1.21\tilde{p}+1\right) \quad (4)$$

where

$$\tilde{p}=1.121\left(1-\sqrt[2.3]{1-e_0\lambda(z)}\right) \quad (5)$$

Now, the maximum modulus of elasticity in the nanocomposite can be written in the following form:

$$E_1=\frac{3}{8}E_\Lambda+\frac{5}{8}E_\Theta \quad (6)$$

where E_Λ and E_Θ are the elastic moduli in the longitudinal and transverse directions that can be obtained as:

$$E_\Lambda=\frac{1+\xi_L\eta_L V_{GPL}}{1-\eta_L V_{GPL}}\times E_M, \quad E_\Theta=\frac{1+\xi_W\eta_W V_{GPL}}{1-\eta_W V_{GPL}}\times E_M \quad (7)$$

where

$$\eta_L=\frac{\left(E_{GPL}/E_M\right)-1}{\left(E_{GPL}/E_M\right)+\xi_L}, \quad \eta_W=\frac{\left(E_{GPL}/E_M\right)-1}{\left(E_{GPL}/E_M\right)+\xi_W} \quad (8)$$

in which E_M and E_{GPL} are related to matrix's elastic moduli and GPLs' elastic moduli, respectively. In addition, V_{GPL} is the GPLs' volume fraction; ξ_L and ξ_W are geometrical coefficients which can be formulated as:

$$\xi_L=\frac{2l_{GPL}}{h_{GPL}}, \quad \xi_W=\frac{2w_{GPL}}{h_{GPL}} \quad (9)$$

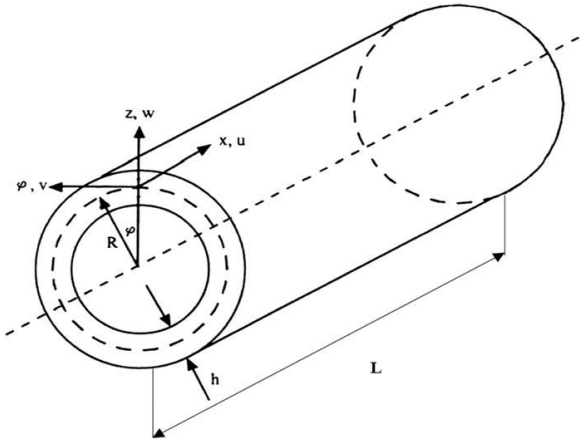

Fig. 1 Geometry and the coordinate system of a cylindrical shell

in the above equation, l_{GPL}, w_{GPL}, and h_{GPL} are the average lengths, width, and thickness of the GPL, respectively. Moreover, the maximum mass density and Poisson's ratio coefficient of the GPLR nanocomposite can be defined as follows:

$$\rho_1=\rho_{GPL}V_{GPL}+\rho_M V_M \quad (10)$$

$$\nu_1=\nu_{GPL}V_{GPL}+\nu_M V_M \quad (11)$$

where V_M stands for the volume fraction of the polymer matrix and can be calculated by V_M=1- V_{GPL}. Moreover, subscript "*e*" stands for the equivalent material properties of the inhomogeneous material. Also, the volume fraction of the GPL can be calculated as:

$$V_{GPL}^*=\frac{g_{GPL}}{g_{GPL}+\left(\rho_{GPL}/\rho_M\right)\left(1-g_{GPL}\right)} \quad (12)$$

in which, g_{GPL} is the weight fraction of the GPLs. Also, the equivalent volume fraction can be separately modified for different porosity distributions as:

$$V_{GPL}=V_{GPL}^*\left[1-\lambda(z)\right] \quad (13)$$

2.2 First-order shear deformable shell theory

The kinematic relations of the nanocomposite shell are going to be derived in this section. The geometry and coordinate system of the structure are shown in Fig. 1. Now, the displacement fields of a shell can be expressed as follows based on the first-order shear deformable shell theory:

$$u_x(x,\varphi,z,t)=u(x,\varphi,t)+z\theta_x(x,\varphi,t),$$
$$u_\varphi(x,\varphi,z,t)=v(x,\varphi,t)+z\theta_\varphi(x,\varphi,t), \quad (14)$$
$$u_z(x,\varphi,z,t)=w(x,\varphi,t)$$

in which u, v and w are axial, circumferential and lateral displacements, respectively. Furthermore, θ_x and θ_φ are the rotation components about axial and circumferential directions, respectively. Henceforward, the nonzero strains

of a shell type element can be written in the following form:

$$\varepsilon_{xx}=\frac{\partial u}{\partial x}+z\frac{\partial \theta_x}{\partial x},\ \ \varepsilon_{\varphi\varphi}=\frac{1}{R}\left(\frac{\partial v}{\partial \varphi}+z\frac{\partial \theta_\varphi}{\partial \varphi}+w\right),$$
$$\varepsilon_{x\varphi}=\frac{1}{R}\frac{\partial u}{\partial \varphi}+\frac{\partial v}{\partial x}+\frac{z}{R}\frac{\partial \theta_x}{\partial \varphi}+z\frac{\partial \theta\varphi}{\partial x}, \tag{15}$$
$$\varepsilon_{xz}=\theta_x+\frac{\partial w}{\partial x},\ \ \varepsilon_{\varphi z}=\theta_\varphi+\frac{1}{R}\frac{\partial w}{\partial \varphi}-\frac{v}{R}$$

2.3 Derivation of motion equations

Herein, the dynamic form of the principle of virtual work, or Hamilton's principle, will be extended for cylindrical shells in order to reach the Euler-Lagrange equations of a nanocomposite shell. Hamilton's principle can be defined in the following form:

$$\int_0^t \delta\left(U-K\right)dt=0 \tag{16}$$

where U and K are strain energy and kinetic energy, respectively. The variation of strain energy for a linear elastic solid can be expressed as:

$$\delta U=\int_{-\frac{h}{2}}^{\frac{h}{2}}\int_0^{2\pi}\int_0^{L}\sigma_{ij}\delta\varepsilon_{ij}R dx d\varphi dz \tag{17}$$

Moreover, the variation of kinetic energy can be written as

$$\delta K=\int_{-\frac{h}{2}}^{\frac{h}{2}}\int_0^{2\pi}\int_0^{L}\rho(z)\left[\left(\frac{\partial \delta u_x}{\partial t}\right)^2+\left(\frac{\partial \delta u_\varphi}{\partial t}\right)^2+\left(\frac{\partial \delta u_z}{\partial t}\right)^2\right]R dx d\varphi dz \tag{18}$$

Now, once Eqs. (17) - (18) are inserted in Eq. (16), the motion equations of cylindrical shells can be written as:

$$\frac{\partial N_{xx}}{\partial x}+\frac{1}{R}\frac{\partial N_{x\varphi}}{\partial \varphi}=I_0\frac{\partial^2 u}{\partial t^2}+I_1\frac{\partial^2 \theta_x}{\partial t^2}, \tag{19}$$

$$\frac{\partial N_{x\varphi}}{\partial x}+\frac{1}{R}\frac{\partial N_{\varphi\varphi}}{\partial \varphi}+\frac{Q_{z\varphi}}{R}=I_0\frac{\partial^2 v}{\partial t^2}+I_1\frac{\partial^2 \theta_\varphi}{\partial t^2}, \tag{20}$$

$$\frac{\partial Q_{xz}}{\partial x}+\frac{1}{R}\frac{\partial Q_{z\varphi}}{\partial \varphi}-\frac{N_{\varphi\varphi}}{R}=I_0\frac{\partial^2 w}{\partial t^2}, \tag{21}$$

$$\frac{\partial M_{xx}}{\partial x}+\frac{1}{R}\frac{\partial M_{x\varphi}}{\partial \varphi}-Q_{xz}=I_1\frac{\partial^2 u}{\partial t^2}+I_2\frac{\partial^2 \theta_x}{\partial t^2}, \tag{22}$$

$$\frac{\partial M_{x\varphi}}{\partial x}+\frac{1}{R}\frac{\partial M_{\varphi\varphi}}{\partial \varphi}-Q_{\varphi z}=I_1\frac{\partial^2 v}{\partial t^2}+I_2\frac{\partial^2 \theta_\varphi}{\partial t^2} \tag{23}$$

where

$$\left[N_{xx},N_{\varphi\varphi},N_{x\varphi}\right]=\int_{-\frac{h}{2}}^{\frac{h}{2}}\left[\sigma_{xx},\sigma_{\varphi\varphi},\sigma_{x\varphi}\right]dz,$$
$$\left[M_{xx},M_{\varphi\varphi},M_{x\varphi}\right]=\int_{-\frac{h}{2}}^{\frac{h}{2}}\left[\sigma_{xx},\sigma_{\varphi\varphi},\sigma_{x\varphi}\right]z dz, \tag{24}$$
$$\left[Q_{xz},Q_{z\varphi}\right]=\kappa_s\int_{-\frac{h}{2}}^{\frac{h}{2}}\left[\sigma_{xz},\sigma_{z\varphi}\right]dz$$

and

$$\left[I_0,I_1,I_2\right]=\int_{-\frac{h}{2}}^{\frac{h}{2}}\left[1,z,z^2\right]\rho(z)dz \tag{25}$$

in which κ_s is shear correction factor.

2.4 Constitutive relations

The stress-strain relationship of a multi-scale hybrid nanocomposite can be expressed in the following form:

$$\sigma_{ij}=C_{ijkl}\varepsilon_{kl} \tag{26}$$

where σ_{ij}, ε_{kl} and C_{ijkl} are components of Cauchy stress, strain and elasticity tensors, respectively. Integrating from above equation over the shell's thickness, the following relation can be achieved:

$$\begin{bmatrix}N_{xx}\\M_{xx}\\N_{\varphi\varphi}\\M_{\varphi\varphi}\end{bmatrix}=\begin{bmatrix}A_{11}&B_{11}&\frac{A_{12}}{R}&\frac{B_{12}}{R}\\B_{11}&D_{11}&\frac{B_{12}}{R}&\frac{D_{12}}{R}\\A_{12}&B_{12}&\frac{A_{11}}{R}&\frac{B_{11}}{R}\\B_{12}&D_{12}&\frac{B_{11}}{R}&\frac{D_{11}}{R}\end{bmatrix}\begin{bmatrix}\frac{\partial u}{\partial x}\\\frac{\partial \theta_x}{\partial x}\\\frac{\partial v}{\partial \varphi}+w\\\frac{\partial \theta_\varphi}{\partial \varphi}\end{bmatrix},$$
$$\begin{bmatrix}N_{x\varphi}\\M_{x\varphi}\end{bmatrix}=\begin{bmatrix}A_{66}&B_{66}\\B_{66}&D_{66}\end{bmatrix}\begin{bmatrix}\frac{1}{R}\frac{\partial u}{\partial \varphi}+\frac{\partial v}{\partial x}\\\frac{1}{R}\frac{\partial \theta_x}{\partial \varphi}+\frac{\partial \theta_\varphi}{\partial x}\end{bmatrix}, \tag{27}$$
$$Q_{xz}=A_{55}^s\left(\theta_x+\frac{\partial w}{\partial x}\right),\ Q_{\varphi z}=A_{55}^s\left(\theta_\varphi+\frac{1}{R}\frac{\partial w}{\partial \varphi}-\frac{v}{R}\right)$$

where

$$\left[A_{11},B_{11},D_{11}\right]=\int_{-\frac{h}{2}}^{\frac{h}{2}}\left[1,z,z^2\right]\frac{E}{1-\nu^2}dz,$$
$$\left[A_{12},B_{12},D_{12}\right]=\int_{-\frac{h}{2}}^{\frac{h}{2}}\left[1,z,z^2\right]\frac{\nu E}{1-\nu^2}dz, \tag{28}$$
$$\left[A_{66},B_{66},D_{66}\right]=\int_{-\frac{h}{2}}^{\frac{h}{2}}\left[1,z,z^2\right]\frac{E}{2(1+\nu)}dz,\ A_{55}^s=\kappa_s\int_{-\frac{h}{2}}^{\frac{h}{2}}\frac{E}{2(1+\nu)}dz$$

2.5 Governing equations

The coupled partial differential governing equations of a multi-scale hybrid nanocomposite shell can be formulated in the following form:

$$A_{11}\frac{\partial^2 u}{\partial x^2}+B_{11}\frac{\partial^2 \theta_x}{\partial x^2}+\frac{A_{12}}{R}\left(\frac{\partial^2 v}{\partial x\partial \varphi}+\frac{\partial w}{\partial x}\right)+$$
$$\frac{B_{12}}{R}\frac{\partial^2 \theta_\varphi}{\partial x\partial \varphi}+\frac{A_{66}}{R}\left(\frac{1}{R}\frac{\partial^2 u}{\partial \varphi^2}+\frac{\partial^2 v}{\partial x\partial \varphi}\right)+\frac{B_{66}}{R}\left(\frac{1}{R}\frac{\partial^2 \theta_x}{\partial \varphi^2}+\frac{\partial^2 \theta_\varphi}{\partial x\partial \varphi}\right) \tag{29}$$
$$-I_0\frac{\partial^2 u}{\partial t^2}-I_1\frac{\partial^2 \theta_x}{\partial t^2}=0,$$

$$A_{66}\left(\frac{1}{R}\frac{\partial^2 u}{\partial x\partial\varphi}+\frac{\partial^2 v}{\partial x^2}\right)+B_{66}\left(\frac{1}{R}\frac{\partial^2\theta_x}{\partial x\partial\varphi}+\frac{\partial^2\theta_\varphi}{\partial x^2}\right)$$
$$+\frac{A_{12}}{R}\frac{\partial^2 u}{\partial x\partial\varphi}+\frac{B_{12}}{R}\frac{\partial^2\theta_x}{\partial x\partial\varphi}+\frac{A_{11}}{R^2}\left(\frac{\partial^2 v}{\partial\varphi^2}+\frac{\partial w}{\partial\varphi}\right)+\frac{B_{11}}{R^2}\frac{\partial^2\theta_\varphi}{\partial\varphi^2}+ \quad (30)$$
$$\frac{A^s_{55}}{R}\left(\theta_\varphi+\frac{1}{R}\frac{\partial w}{\partial\varphi}-\frac{v}{R}\right)-I_0\frac{\partial^2 v}{\partial t^2}-I_1\frac{\partial^2\theta_\varphi}{\partial t^2}=0,$$

$$A^s_{55}\left(\frac{\partial\theta_x}{\partial x}+\frac{\partial^2 w}{\partial x^2}\right)+\frac{A^s_{55}}{R}\left(\frac{\partial\theta_\varphi}{\partial\varphi}+\frac{1}{R}\frac{\partial^2 w}{\partial\varphi^2}-\frac{1}{R}\frac{\partial v}{\partial\varphi}\right)$$
$$-\frac{A_{12}}{R}\frac{\partial u}{\partial x}-\frac{B_{12}}{R}\frac{\partial\theta_x}{\partial x}-\frac{A_{11}}{R^2}\left(\frac{\partial v}{\partial\varphi}+w\right)-\frac{B_{11}}{R^2}\frac{\partial\theta_\varphi}{\partial\varphi}-I_0\frac{\partial^2 w}{\partial t^2}=0, \quad (31)$$

$$B_{11}\frac{\partial^2 u}{\partial x^2}+D_{11}\frac{\partial^2\theta_x}{\partial x^2}+\frac{B_{12}}{R}\left(\frac{\partial^2 v}{\partial x\partial\varphi}+\frac{\partial w}{\partial x}\right)$$
$$+\frac{D_{12}}{R}\frac{\partial^2\theta_\varphi}{\partial x\partial\varphi}+\frac{B_{66}}{R}\left(\frac{1}{R}\frac{\partial^2 u}{\partial\varphi^2}+\frac{\partial^2 v}{\partial x\partial\varphi}\right)+\frac{D_{66}}{R}\left(\frac{1}{R}\frac{\partial^2\theta_x}{\partial\varphi^2}+\frac{\partial^2\theta_\varphi}{\partial x\partial\varphi}\right) \quad (32)$$
$$-A^s_{55}\left(\theta_x+\frac{\partial w}{\partial x}\right)-I_1\frac{\partial^2 u}{\partial t^2}-I_2\frac{\partial^2\theta_x}{\partial t^2}=0,$$

$$B_{66}\left(\frac{1}{R}\frac{\partial^2 u}{\partial x\partial\varphi}+\frac{\partial^2 v}{\partial x^2}\right)+D_{66}\left(\frac{1}{R}\frac{\partial^2\theta_x}{\partial x\partial\varphi}+\frac{\partial^2\theta_\varphi}{\partial x^2}\right)$$
$$+\frac{B_{12}}{R}\frac{\partial^2 u}{\partial x\partial\varphi}+\frac{D_{12}}{R}\frac{\partial^2\theta_x}{\partial x\partial\varphi}+\frac{B_{11}}{R^2}\left(\frac{\partial^2 v}{\partial\varphi^2}+\frac{\partial w}{\partial\varphi}\right)+\frac{D_{11}}{R^2}\frac{\partial^2\theta_\varphi}{\partial\varphi^2}- \quad (33)$$
$$A^s_{55}\left(\theta_\varphi+\frac{1}{R}\frac{\partial w}{\partial\varphi}-\frac{v}{R}\right)-I_1\frac{\partial^2 v}{\partial t^2}-I_2\frac{\partial^2\theta_\varphi}{\partial t^2}=0$$

3. Solution procedure

The present section is dedicated to solve the achieved partial differential governing equations of the problem. To reach this purpose, the displacement field's components are assumed to possess exponential solutions as follows:

$$\begin{aligned}
u(x,\varphi,t)&=U\exp\left(i\left[\beta x+n\varphi-\omega t\right]\right),\\
v(x,\varphi,t)&=V\exp\left(i\left[\beta x+n\varphi-\omega t\right]\right),\\
w(x,\varphi,t)&=W\exp\left(i\left[\beta x+n\varphi-\omega t\right]\right),\\
\theta_x(x,\varphi,t)&=\Theta_x\exp\left(i\left[\beta x+n\varphi-\omega t\right]\right),\\
\theta_\varphi(x,\varphi,t)&=\Theta_\varphi\exp\left(i\left[\beta x+n\varphi-\omega t\right]\right)
\end{aligned} \quad (34)$$

where β and n are axial and circumferential wave numbers, respectively and ω is the circular frequency. Once Eq. (34) is inserted in Eqs. (29) - (33), the following eigenvalue equation is obtained:

$$\left(\mathbf{K}-\omega^2\mathbf{M}\right)\{\mathbf{\Delta}\}=\mathbf{0} \quad (35)$$

where **K** and **M** are stiffness and mass matrices, respectively and **Δ** denotes a column vector containing the wave amplitudes (U, V, W, Θ_x, Θ_φ). The frequency of the dispersed waves can be easily computed by solving Eq. (35) for ω. This process can be performed by setting the determinant of the left-hand-side of Eq. (35) equal to zero:

$$\left|\mathbf{K}-\omega^2\mathbf{M}\right|=0 \quad (36)$$

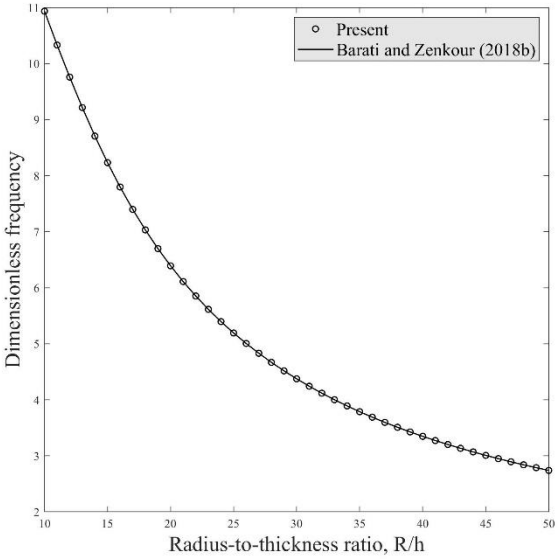

Fig. 2 Comparison of the first dimensionless frequency of GPLR nanocomposite S-S shells (W_{GPL}=1%, L/h=20)

Afterward, the velocity of the propagated waves can be calculated via:

$$c_p=\frac{\omega}{\beta} \quad (37)$$

4. Numerical results and discussion

In this section, a group of numerical results will be rendered in order to clarify the influence of each parameter on the wave dispersion behaviors of GPLR nanocomposite shells. The material properties are chosen just as same as those implemented by Barati and Zenkour (2018b). Also, the validity of the presented methodology is shown in Fig. 2 comparing the results of our modeling with those reported by Barati and Zenkour (2018b). The presented diagram reveals that the presented method is able to estimate exact frequency responses. In the future numerical illustrations, the dimensionless form of the wave frequency is rendered which can be calculated by:

$$\Omega=100\omega h\sqrt{\frac{\rho_M}{E_M}} \quad (38)$$

Variation of dimensionless wave frequency for two types of porosity distribution of GPL reinforced shells versus radius-to-thickness ratio for different longitudinal wave numbers are indicated in Fig. 3 at n=2, W_{GPL}=1%, e_0=0.4. In β=1(1/m) Asymmetric distribution has higher dimensionless wave frequencies than symmetric distribution. Asymmetric distribution and symmetric distribution have the same results and dimensionless wave frequencies (β=10(1/m)). In Fig. 3c, at first asymmetric distribution, has the same dimensionless wave frequency with symmetric distribution but gradually dimensionless wave frequencies of asymmetric distribution become smaller than symmetric distribution. In other words, by

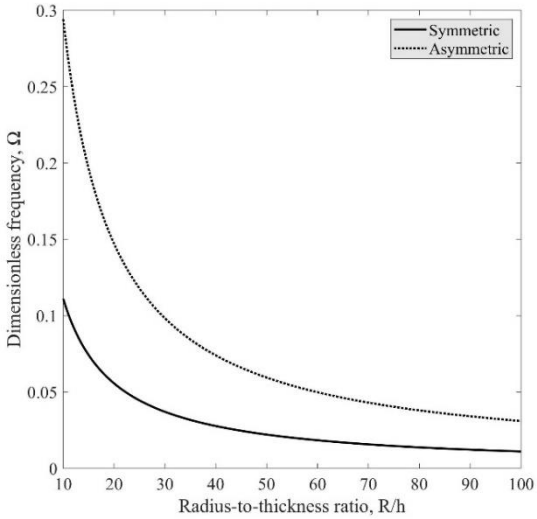

(a) β=1 (1/m)

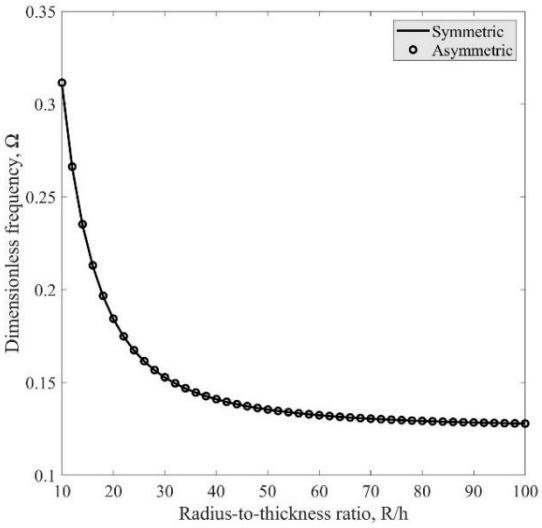

(b) β=10 (1/m)

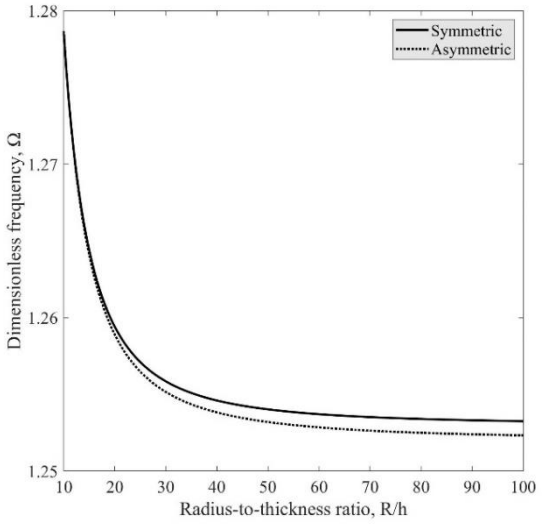

(c) β=100 (1/m)

Fig. 3 Illustration of coupled effects of longitudinal wave number and porosity distribution on the variations of dimensionless wave frequency of GPL reinforced shells versus radius-to-thickness ratio (n=2, W_{GPL}=1%, e_0=0.4)

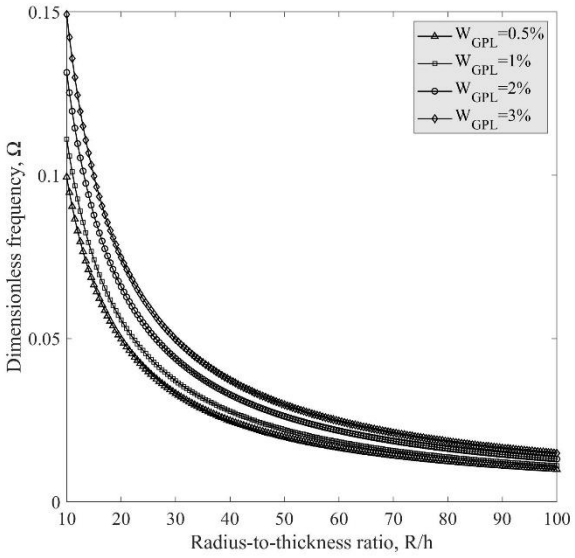

Fig. 4 Variation of dimensionless wave frequency versus radius-to-thickness ratio for various weight fractions of GPLs by considering symmetric porosity distribution (n=2, β=1, e0=0.4)

rising longitudinal wave number, asymmetric frequencies become smaller than symmetric frequencies. Also, with increasing radius-to-thickness ratio the dimensionless wave frequencies are reduced. Nanocomposite shells with higher radius-to-thickness ratio reveal such a behavior owing to their greater flexibility.

Fig. 4 demonstrates the effects of GPLs' weight fraction on changes of dimensionless wave frequency versus radius-to-thickness ratio by considering symmetric porosity distribution (n=2, β=1, e_0=0.4). It is obvious that nanocomposite shells with a higher weight fraction of GPLs have higher dimensionless wave frequencies. It means if a small amount of GPL is dispersed into the matrix, the effective stiffness of the porous shell is increased. Also, it can be figured out that the structure becomes softer as the radius-to-thickness ratio increases and this trend lessens the system's frequency in a continuous manner.

Mixed effects of longitudinal wave number and GPLs' weight fraction on the dimensionless wave frequency of porous shells versus circumferential wave number are presented in Fig. 5 by considering symmetric porosity distribution (R/h=20, e_0=0.4). It can be observed that by adding the value of the circumferential wave number, the dimensionless frequency enlarges. According to Fig. 5, the dimensionless wave frequency in each weight fraction is increased by increasing the circumferential wave number. Besides, nanocomposite shells with higher GPLs' weight fraction have higher dimensionless wave frequencies. In other words, by rising GPLs' weight fraction, the dimensionless wave frequency increases. In addition, dimensionless wave frequency can be aggrandized whenever a higher value is assigned to the longitudinal wave number.

Furthermore, the influences of different porosity coefficients on the wave frequency curves of

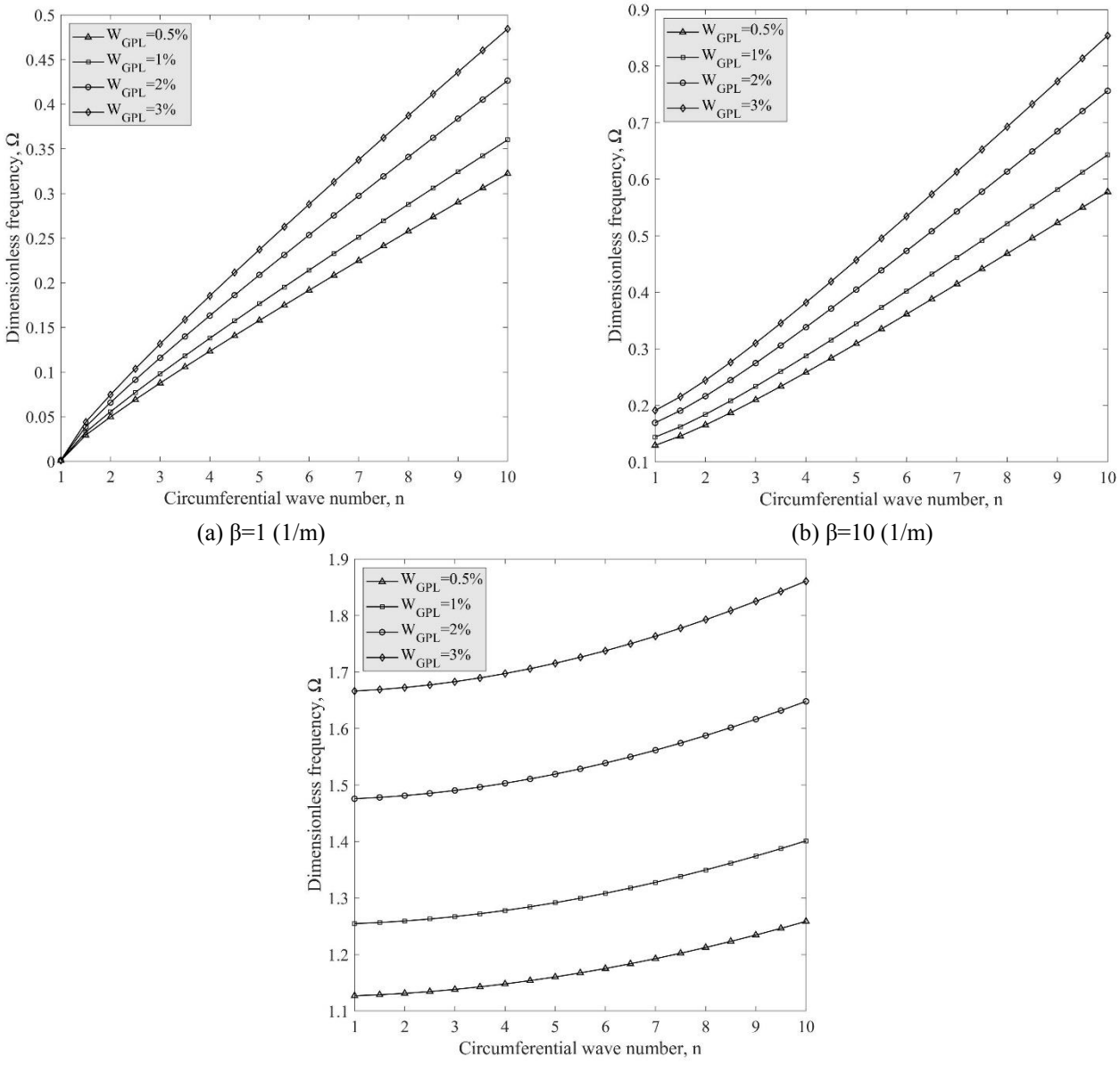

(a) β=1 (1/m)

(b) β=10 (1/m)

(c) β=100 (1/m)

Fig. 5 Illustration of coupled effects of both circumferential and longitudinal wave numbers and GPLs' weight fraction on the dimensionless wave frequency of porous shells using symmetric distribution for porosity (R/h=20, e_0=0.4)

nanocomposite shells are shown in Fig. 6 considering symmetric porosity distribution (R/h=20, n=2, β=1). Clearly, perfect structures (e_0=0) possess higher amounts of dimensionless wave frequency in comparison with porous structures (nonzero porosity coefficients). In other words, an increase in the coefficient of porosity results in observing lower dimensionless wave frequencies. Also, again it can be found that the mechanical frequency becomes greater in the cases which a higher weight fraction is chosen for the GPLs.

Finally, Fig. 7 depicts the variation of phase velocity versus weight fraction of GPLs for different porosity coefficients for GPLR porous nanocomposites with symmetric porosity distribution. Based on Fig. 7, it can be concluded that for all kind of porosity coefficient whenever the GPLs' weight fraction increases, the phase velocity of porous shell increases, too. It can be seen that in a constant value of GPLs' weight fraction, the growth of the porosity coefficient leads to a decrease in the phase velocity. Indeed, perfect nanocomposite shells have the highest value of phase velocity.

5. Conclusion

This paper was majorly performed to analytically investigate the wave dispersion behaviors of GPLR nanocomposite cylinders with respect to the porosity effects. Governing equations were developed on the basis of the dynamic form of the virtual work's principle. The effective material properties were achieved using the Halpin-Tsai micromechanical scheme. Herein, the most crucial concluding remarks are going to be reviewed:

- The porosity affects the material properties in the

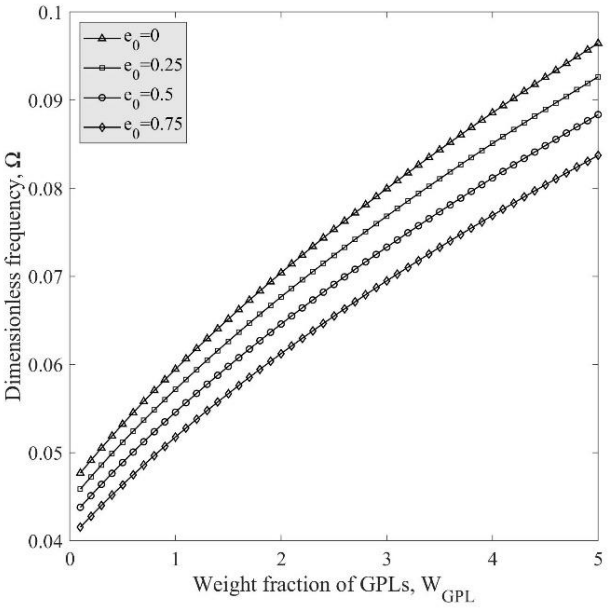

Fig. 6. Variation of dimensionless wave frequency versus GPLs' weight fraction for different porosity coefficients by considering symmetric porosity distribution (R/h=20, n=2, β=1)

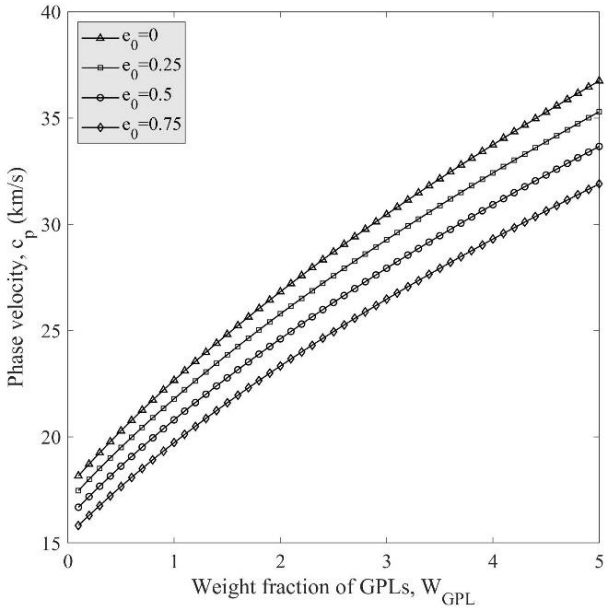

Fig. 7 Variation of phase velocity versus GPLs' weight fraction for different porosity coefficients by considering symmetric porosity distribution (R/h=20, n=2, β=1)

way that the porous structures possess lower frequencies in comparison with the perfect ones.

• The stiffness of the cylinder can be added if the weight fraction of GPLs is increased and hence, the wave frequency can be increased in such a condition.

• Wave frequency and phase velocity can be decreased once the radius-to-thickness ratio is added.

• In small longitudinal wave numbers, symmetric distribution of the porosity lessens the mechanical frequency more than asymmetric type; however, this trend can be observed reversely once a great longitudinal wave number is selected.

References

Akbaş, S.D. (2018), "Bending of a cracked functionally graded nanobeam", *Adv. Nano Res.*, **6**(3), 219-242. https://doi.org/10.12989/anr.2018.6.3.219.

Akgöz, B. and Civalek, Ö. (2014), "A new trigonometric beam model for buckling of strain gradient microbeams", *J. Mech. Sci.,* **81**, 88-94. https://doi.org/10.1016/j.ijmecsci.2014.02.013.

Akgöz, B. and Civalek, Ö. (2015a), "A microstructure-dependent sinusoidal plate model based on the strain gradient elasticity theory", *Acta Mechanica,* **226**, 2277-2294. https://doi.org/10.1007/s00707-015-1308-4.

Akgöz, B. and Civalek, Ö. (2015b), "A novel microstructure-dependent shear deformable beam model", *J. Mech. Sci.,* **99**, 10-20. https://doi.org/10.1016/j.ijmecsci.2015.05.003

Ansari, R., Shojaei, M.F., Mohammadi, V., Gholami, R. and Sadeghi, F. (2014), "Nonlinear forced vibration analysis of functionally graded carbon nanotube-reinforced composite timoshenko beams", *Compos. Struct.,* **113**, 316-327. https://doi.org/10.1016/j.compstruct.2014.03.015.

Barati, M.R. and Zenkour, A.M. (2017), "Post-buckling analysis of refined shear deformable graphene platelet reinforced beams with porosities and geometrical imperfection", *Compos. Struct.,* **181**, 194-202. https://doi.org/10.1016/j.compstruct.2017.08.082.

Barati, M.R. and Zenkour, A.M. (2018a), "Analysis of postbuckling of graded porous gpl-reinforced beams with geometrical imperfection", *Mech. Adv. Mater. Struct.*, 1-9. https://doi.org/10.1080/15376494.2017.1400622.

Barati, M.R. and Zenkour, A.M. (2018b), "Vibration analysis of functionally graded graphene platelet reinforced cylindrical shells with different porosity distributions", *Mech. Adv. Mater. Struct.,* 1-9. https://doi.org/10.1080/15376494.2018.1444235.

Civalek, Ö. (2017), "Free vibration of carbon nanotubes reinforced (cntr) and functionally graded shells and plates based on fsdt via discrete singular convolution method", *Compos. Part B,* **111**, 45-59. https://doi.org/10.1016/j.compositesb.2016.11.030.

Ebrahimi, F. and Barati, M.R. (2017a), "Flexural wave propagation analysis of embedded s-fgm nanobeams under longitudinal magnetic field based on nonlocal strain gradient theory", *Arabian J. Sci. Eng.,* **42**, 1715-1726. https://doi.org/10.1007/s13369-016-2266-4.

Ebrahimi, F. and Barati, M.R. (2017b), "Through-the-length temperature distribution effects on thermal vibration analysis of nonlocal strain-gradient axially graded nanobeams subjected to nonuniform magnetic field", *J. Themral Stresses,* **40**(5), 548-563. https://doi.org/10.1080/01495739.2016.1254076.

Ebrahimi, F. and Barati, M.R. (2018), "Vibration analysis of piezoelectrically actuated curved nanosize FG beams via a nonlocal strain-electric field gradient theory", *Mech. Adv. Mater. Struct.,* **25**, 350-359. https://doi.org/10.1080/15376494.2016.1255830.

Ebrahimi, F. and Dabbagh, A. (2017a), "Nonlocal strain gradient based wave dispersion behavior of smart rotating magneto-electro-elastic nanoplates", *Mater. Res. Express,* **4**. https://doi.org/10.1088/2053-1591/aa55b5.

Ebrahimi, F. and Dabbagh, A. (2017b), "Wave propagation analysis of smart rotating porous heterogeneous piezo-electric nanobeams", *European Phys. J. Plus,* **132**, 153. https://doi.org/10.1140/epjp/i2017-11366-3.

Ebrahimi, F., Barati, M.R. and Haghi, P. (2017), "Thermal effects on wave propagation characteristics of rotating strain gradient temperature-dependent functionally graded nanoscale beams", *J. Themral Stresses,* **40**, 535-547.

https://doi.org/10.1080/01495739.2016.1230483.

Ebrahimi, F., Barati, M.R. and Haghi, P. (2018), "Wave propagation analysis of size-dependent rotating inhomogeneous nanobeams based on nonlocal elasticity theory", *J. Vib. Control,* **24**, 3809-3818. https://doi.org/10.1177%2F1077546317711537.

Ebrahimi, F., Dehghan, M. and Seyfi, A. (2019), "Eringen's nonlocal elasticity theory for wave propagation analysis of magneto-electro-elastic nanotubes", *Adv. Nano Res.,* **7**, 1-11. https://doi.org/10.12989/anr.2019.7.1.001.

Feng, C., Kitipornchai, S. and Yang, J. (2017a), "Nonlinear bending of polymer nanocomposite beams reinforced with non-uniformly distributed graphene platelets (gpls)", *Compos. Part B,* **110**, 132-140. https://doi.org/10.1016/j.compositesb.2016.11.024.

Feng, C., Kitipornchai, S. and Yang, J. (2017b), "Nonlinear free vibration of functionally graded polymer composite beams reinforced with graphene nanoplatelets (gpls)", *Eng. Struct.,* **140**, 110-119. https://doi.org/10.1016/j.engstruct.2017.02.052.

Kaci, A., Houari, M.S.A., Bousahla, A.A., Tounsi, A. and Mahmoud, S. (2018), "Post-buckling analysis of shear-deformable composite beams using a novel simple two-unknown beam theory", *Struct. Eng. Mech.,* **65**, 621-631. https://doi.org/10.12989/sem.2018.65.5.621.

Ke, L.L., Yang, J. and Kitipornchai, S. (2010), "Nonlinear free vibration of functionally graded carbon nanotube-reinforced composite beams", *Compos. Struct.,* **92**, 676-683. https://doi.org/10.1016/j.compstruct.2009.09.024.

Khetir, H., Bouiadjra, M.B., Houari, M.S.A., Tounsi, A. and Mahmoud, S. (2017), "A new nonlocal trigonometric shear deformation theory for thermal buckling analysis of embedded nanosize FG plates", *Struct. Eng. Mech.,* **64**, 391-402. http://dx.doi.org/10.12989/sem.2017.64.4.391.

Kitipornchai, S., Chen, D. and Yang, J. (2017), "Free vibration and elastic buckling of functionally graded porous beams reinforced by graphene platelets", *Mater. Design,* **116**, 656-665. https://doi.org/10.1016/j.matdes.2016.12.061.

Kocaturk, T. and Akbas, S.D. (2013), "Wave propagation in a microbeam based on the modified couple stress theory", *Struct. Eng. Mech.,* **46**, 417-431. https://doi.org/10.12989/sem.2013.46.3.417.

Pour, H.R., Vossough, H., Heydari, M.M., Beygipoor, G. and Azimzadeh, A. (2015), "Nonlinear vibration analysis of a nonlocal sinusoidal shear deformation carbon nanotube using differential quadrature method", *Struct. Eng. Mech.,* **54**, 1061-1073. http://dx.doi.org/10.12989/sem.2015.54.6.1061.

Reddy, R.M.R., Karunasena, W. and Lokuge, W. (2018), "Free vibration of functionally graded-gpl reinforced composite plates with different boundary conditions", *Aerosp. Sci. Technol.,* **78**, 147-156. https://doi.org/10.1016/j.ast.2018.04.019.

Rout, M. and Karmakar, A. (2018), "Free vibration of rotating pretwisted cnts-reinforced shallow shells in thermal environment", *Mech. Adv. Mater. Struct.*, 1-13. https://doi.org/10.1080/15376494.2018.1452317.

Shen, H.S. and Xiang, Y. (2014), "Postbuckling of axially compressed nanotube-reinforced composite cylindrical panels resting on elastic foundations in thermal environments", *Compos. B,* **67**, 50-61. https://doi.org/10.1016/j.compositesb.2014.06.020.

Song, M., Kitipornchai, S. and Yang, J. (2017a), "Free and forced vibrations of functionally graded polymer composite plates reinforced with graphene nanoplatelets", *Compos. Struct.,* **159**, 579-588. https://doi.org/10.1016/j.compstruct.2016.09.070.

Song, M., Yang, J. and Ktipornchai, S. (2018), "Bending and buckling analyses of functionally graded polymer composite plates reinforced with graphene nanoplatelets", *Compos. B,* **134**, 106-113. https://doi.org/10.1016/j.compositesb.2017.09.043

Song, M., Yang, J., Kitipornchai, S. and Zhu, W. (2017b), "Buckling and postbuckling of biaxially compressed functionally graded multilayer graphene nanoplatelet-reinforced polymer composite plates", *J. Mech. Sci.,* **131**, 345-355. https://doi.org/10.1016/j.ijmecsci.2017.07.017.

Wang, A., Chen, H., Hao, Y. and Zhang, W. (2018a), "Vibration and bending behavior of functionally graded nanocomposite doubly-curved shallow shells reinforced by graphene nanoplatelets", *Results in Phys.,* **9**, 550-559. https://doi.org/10.1016/j.rinp.2018.02.062.

Wang, Q., Cui, X., Qin, B. and Liang, Q. (2017), "Vibration analysis of the functionally graded carbon nanotube reinforced composite shallow shells with arbitrary boundary conditions", *Compos. Struct.,* **182**, 364-379.

Wang, Y., Feng, C., Zhao, Z. and Yang, J. (2018c), "Buckling of graphene platelet reinforced composite cylindrical shell with cutout", *J. Struct. Stability Dynam.,* **18**, https://doi.org/10.1142/S0219455418500402.

Wang, Y., Feng, C., Zhao, Z. and Yang, J. (2018d), "Eigenvalue buckling of functionally graded cylindrical shells reinforced with graphene platelets (gpl)", *Compos. Struct.,* **202**, 38-46. https://doi.org/10.1016/j.compstruct.2017.10.005.

Wang, Y., Feng, C., Zhao, Z., Lu, F. and Yang, J. (2018b), "Torsional buckling of graphene platelets (gpls) reinforced functionally graded cylindrical shell with cutout", *Compos. Struct.,* **197**, 72-79.

Yang, J., Wu, H. and Kitipornchai, S. (2017), "Buckling and postbuckling of functionally graded multilayer graphene platelet-reinforced composite beams", *Compos. Struct.,* **161**, 111-118. https://doi.org/10.1016/j.compstruct.2016.11.048.

Zhang, L., Song, Z. and Liew, K. (2015), "Nonlinear bending analysis of fg-cnt reinforced composite thick plates resting on pasternak foundations using the element-free imls-ritz method", *Compos. Struct.,* **128**, 165-175. https://doi.org/10.1016/j.compstruct.2015.03.011.

Zhao, Z., Feng, C., Wang, Y. and Yang, J. (2017), "Bending and vibration analysis of functionally graded trapezoidal nanocomposite plates reinforced with graphene nanoplatelets (gpls)", *Compos. Struct.,* **180**, 799-808. https://doi.org/10.1016/j.compstruct.2017.08.044.

Zhu, P., Lei, Z. and Liew, K.M. (2012), "Static and free vibration analyses of carbon nanotube-reinforced composite plates using finite element method with first order shear deformation plate theory", *Compos. Struct.,* **94**, 1450-1460. https://doi.org/10.1016/j.compstruct.2011.11.010.

Zidi, M., Houari, M.S.A., Tounsi, A., Bessaim, A. and Mahmoud, S. (2017), "A novel simple two-unknown hyperbolic shear deformation theory for functionally graded beams", *Struct. Eng. Mech.,* **64**, 145-153. http://dx.doi.org/10.12989/sem.2017.64.2.145.

CC